Supporting Information

Mono- and hexa-Palladium doped silver nanoclusters stabilized by dithiolates

Subrat Kumar Barik,[a] Tzu-Hao Chiu,[a] Yu-Chiao Liu,[b] Ming-Hsi Chiang,*[b] Franck Gam,[c] Isaac Chantrenne,[c] Samia Kahlal,[c] Jean-Yves Saillard,*[c] and C. W. Liu*[a]

[a]Department of Chemistry, National Dong Hwa University, Hualien 97401, Taiwan (R.O.C.)

[b]Institute of Chemistry, Academia Sinica, Taipei 11528, Taiwan (R.O.C.)

[c]Univ Rennes, CNRS, ISCR – UMR 6226, F–35000 Rennes, France

*To whom correspondence should be addressed. Email: *chenwei@mail.ndhu.edu.tw*

Table of Contents

I. Experimental Details

I.1 Materials and Methods

All the reactions were conducted under an Ar/N_2 atmosphere using standard Schlenk technique. The solvents were distilled under N_2 atmosphere prior to use. $[Ag(CH_3CN)_4](PF_6)$,[1] $Pd[S_2P(O^nPr)_2]_2$[2] and $NH_4[S_2P(O^nPr)_2]$[3] ligand were prepared as described in the literature. $LiBH_4$ (2M in THF) and all other chemicals were purchased from commercial sources and were used as received. Preparative thin-layer chromatography was performed with Merck 105554 TLC Silica gel 60 F_{254}, layer thickness 250 µm on aluminum sheets (20 x 20 cm). NMR spectra were recorded on Bruker Advance DPX300 FT-NMR spectrometer that operates at 300 and 400 MHz while recording ^1H, 121.5 and 161.9 MHz, respectively for ^{31}P. Residual solvent protons were used as a reference (δ, ppm, $CDCl_3$, 7.26). ^{31}P NMR spectra were referenced to external 85% H_3PO_4 at δ 0.00. ESI-mass spectra were recorded on a Fison Quattro Bio-Q (Fisons Instruments, VG Biotech, UK). Melting points were measured by using a Fargo MP-2D melting point apparatus. The elemental analyses were done using a Perkin-Elmer 2400 CHN analyzer. The elemental and structural information were analyzed using x-ray photoelectron spectrometer (XPS, VG Multilab 2000-Thermo Scientific Inc. UK, Kα) with a microfocus monochromated Al Kα X-ray working with high photonic energies from 0.2 to 3 KeV. UV–Visible absorption spectra were measured on a Perkin Elmer Lambda 750 spectrophotometer using quartz cells with path length of 1 cm. Electrochemical measurements were recorded on a CH Instruments 733B electrochemical potentiostat using a gastight three-electrode cell under N_2. A vitreous carbon electrode (1 mm in diameter) and a platinum wire were used as the working and auxiliary electrodes, respectively. The reference electrode was a nonaqueous Ag^+/Ag electrode (0.01 M $AgNO_3$/0.1 M $[nBu_4N][BArF_{24}]$, $BArF_{24}^- = B(3,5\text{-}C_6H_3(CF_3)_2)_4^-$). All potentials were measured in CH_2Cl_2 solution containing 0.1 M $[nBu_4N][BArF_{24}]$. The sample concentration of **1** and **2** were 0.6 and 0.55 mM. The potentials are reported against the ferrocenium/ferrocene (Fc^+/Fc) couple.

I.2 Synthetic Section

Synthesis of [PdAg$_{20}${S$_2$P(O^{n}Pr)$_2$}$_{12}$] (1)

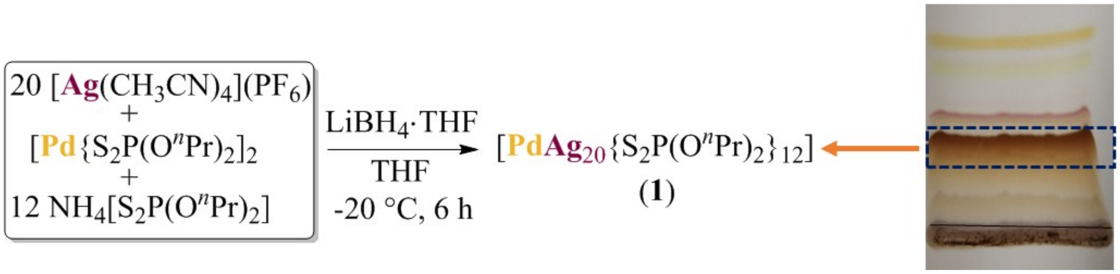

Scheme 1. Synthesis of **1**.

In a flame dried Schlenk flask, [Ag(CH$_3$CN)$_4$](PF$_6$) (0.164 g, 0.394 mmol) was suspended in THF (15 mL). To this NH$_4$[S$_2$P(O^{n}Pr)$_2$] (0.055 g, 0.236 mmol), [Pd{S$_2$P(O^{n}Pr)$_2$}] (0.0105 g, 0.0197 mmol) were added. Then the reaction flask was kept at -20 ºC for 10 minutes. LiBH$_4$·THF (0.5 mL, 1.0 mmol) was added slowly to the reaction mixture and then the resulting mixture was stirred at -20 ºC for 6 hours. The color of the solution turned orange to black after the LiBH$_4$·THF addition. The solvent was evaporated under vacuum and residue was washed with deionized water to remove decomposed impurities from ligand and extracted in CH$_2$Cl$_2$. The resulting CH$_2$Cl$_2$ solution was dried and the residue was further dissolved in hexane. The mother liquor was concentrated and was chromatographed on silica gel TLC plates. Elution with a hexane/CH$_2$Cl$_2$ (40:60 *v/v*) mixture resulted brown-red compound [Ag$_{20}$Pd{S$_2$P(O^{n}Pr)$_2$}$_{12}$], **1** (0.032 g, 34 % yield, based on Pd).

1: Mp: 185 °C (dec.). ESI-MS = *m/z* 4930.8 [M+Ag]$^+$ (Calcd. 4930.9). ^{1}H NMR (22 °C, 300 MHz, CDCl$_3$, δ, ppm): 4.14-4.07 (q, 48H, OCH_2), 1.79-1.67 (m, 48H, CH_2), 0.97-0.92 (t, 72H, CH_3). ^{31}P NMR (22 °C, 121.49 MHz, CDCl$_3$, δ, ppm): 104.9. UV-vis [λ_{max} in nm, (ε in M^{-1}cm^{-1})] 384 (36324), 436 (47613), 477 (32377). Anal. Cald for C$_{72}$H$_{168}$PdAg$_{20}$S$_{24}$O$_{24}$P$_{12}$·C$_4$H$_8$O: C, 18.64, H, 3.62; S, 15.72 Found C, 18.74, H, 3.71; S, 15.37.

Synthesis of $[Pd_6Ag_{14}S\{S_2P(O^nPr)_2\}_{12}]$ (2)

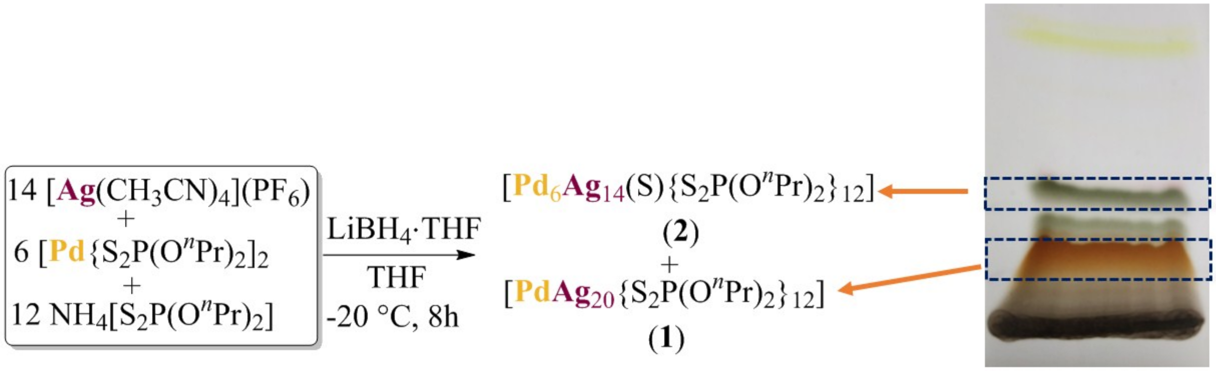

Scheme 2. Synthesis of compound **2**.

In a flame dried Schlenk flask, $[Ag(CH_3CN)_4](PF_6)$ (0.15 g, 0.349 mmol) was suspended in THF (15 mL). To this $NH_4[S_2P(O^nPr)_2]$ (0.069 g, 0.3 mmol), $[Pd\{S_2P(O^nPr)_2\}]$ (0.080 g, 0.150 mmol) were added. Then the reaction flask was kept at -20 ºC for 10 minutes. $LiBH_4$·THF (0.4 mL, 0.8 mmol) was added slowly to the reaction mixture and then the resulting mixture was stirred at -20 ºC for 8 hours. The color of the solution turned orange to black after the $LiBH_4$·THF addition. The solvent was evaporated under vacuum and residue was washed with deionized water to remove decomposed impurities from ligand and extracted in CH_2Cl_2. The resulting CH_2Cl_2 solution was concentrated and subjected to thin layer chromatography. Elution with a hexane/CH_2Cl_2 (40:60 *v/v*) mixture resulted dark green compound $[Pd_6Ag_{14}(S)\{S_2P(O^nPr)_2\}_{12}]$, **2** from the reaction mixture (0.026 g, 22 % yield, based on Pd). Note that several stoichiometry and conditions were adopted for the synthesis of **2,** however we found the given reaction condition is the suitable one.

2: Mp: 173 °C (dec.). ESI-MS = *m*/*z* 4848.2 $[M+Ag]^+$ (Calcd. 4847.9). ^{1}H NMR (22 °C, 400 MHz, $CDCl_3$, δ, ppm): 4.29-3.89 (m, 48H, OCH_2), 1.78-1.69 (m, 48H, CH_2) and 0.98-0.94 (t, 72H, CH_3). ^{31}P NMR (22 °C, 161.9 MHz, $CDCl_3$, δ, ppm): 104.3 and 100.1. UV-vis [λ_{max} in nm, (ε in $M^{-1}cm^{-1}$)] 291 (41930), 370 (26530), 375 (17820), 406 (17230), 443 (17070), 548 (11620) 618 (11690) Anal. Cald for $C_{72}H_{168}Pd_6Ag_{14}S_{25}O_{24}P_{12}$: C, 18.24, H, 3.57; S, 16.91 Found C, 18.54, H, 3.42; S, 16.97.

I.3 X-Ray analysis Details

Single crystals suitable for X-ray diffraction analysis of **1** and **2** were obtained by diffusing hexane into concentrated CH_2Cl_2 solution at room temperature within a week. The single crystals were mounted on the tip of glass fiber coated in paratone oil, then frozen at 150 K. Data were collected on a Bruker APEX II CCD diffractometer using graphite monochromated Mo Kα radiation (λ = 0.71073 Å). Absorption corrections for area detector were performed with SADABS[4] and the integration of raw data frame was performed with SAINT[5]. The structure was solved by direct methods and refined by least-squares against F^2 using the SHELXL-2018/3 package,[6,7] incorporated in SHELXTL/PC V6.14.[8] All non-hydrogen atoms were refined anisotropically. The structure reported herein has been deposited at the Cambridge Crystallographic Data Centre, CCDC 1911605 (**1**) and CCDC 1911606 (**2**). Selected crystallographic data is listed in Table S1.

I.4 Computational Details

Geometry optimizations were performed by density functional theory (DFT) calculations with the Gaussian 16 package,[9] using the BP86 functional[10] and the all-electron Def2-TZVP set from EMSL Basis Set Exchange Library.[11] In the case of compound **2'**, calculations were also performed with the inclusion of the 3-parameter Grimme's empirical corrections (GD3BJ) for dispersion forces. [12] For the sake of comparison with **1'** and previously published isoelectronic clusters, these calculations are not discussed in the manuscript, but relevant interatomic distances provided in Table S2. In any case, the results obtained on **2'** with and without considering Grimme's corrections are not very different.

All the optimized geometries were characterized as true minima by vibrational analysis. The NAO charges and Wiberg bond indices were computed with the NBO 6.0 program[13] on single-point calculations performed with the BP86 functional and the Def2-SVP basis set for computational limitations.[14] The DFT-computed electrochemical HOMO-LUMO gaps were obtained from the ionization potentials and electron affinities of **1'** and **2'** calculated in CH_2Cl_2, the solvent effect being considered within the PCM model.[15] The UV-visible transitions were calculated by means of time-dependent DFT (TD-DFT) calculations, with the CAM-B3LYP functional[16] and the Def2-TZVP basis set. Only singlet-singlet, *i.e.* spin-allowed, transitions have been computed. The UV-visible spectra were simulated from the computed TD-DFT transitions and their oscillator strengths by using the SWizard program,[17] each transition is associated with a Gaussian function of half-height width equal to 3000 cm^{-1}. The compositions of the molecular orbitals were calculated using the AOMix program.[18]

II Supplementary Data

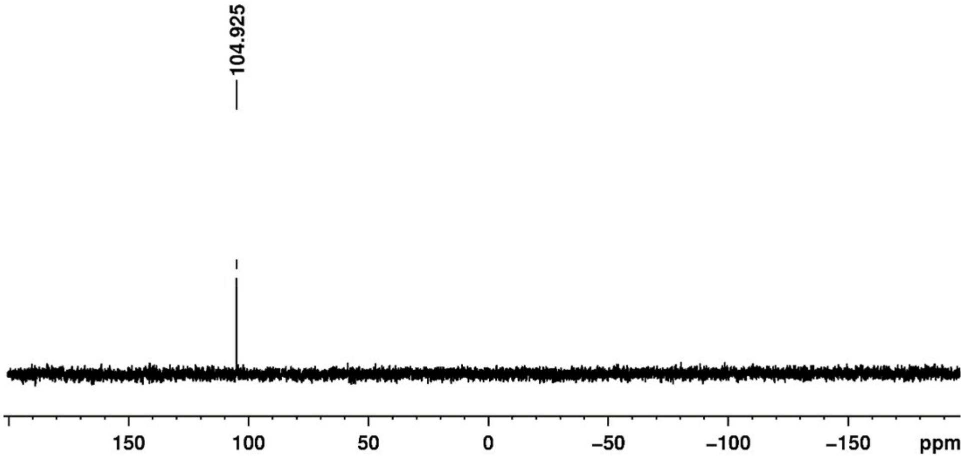

Figure S1. ^{31}P NMR spectrum of **1** (121.9 MHz, $CDCl_3$).

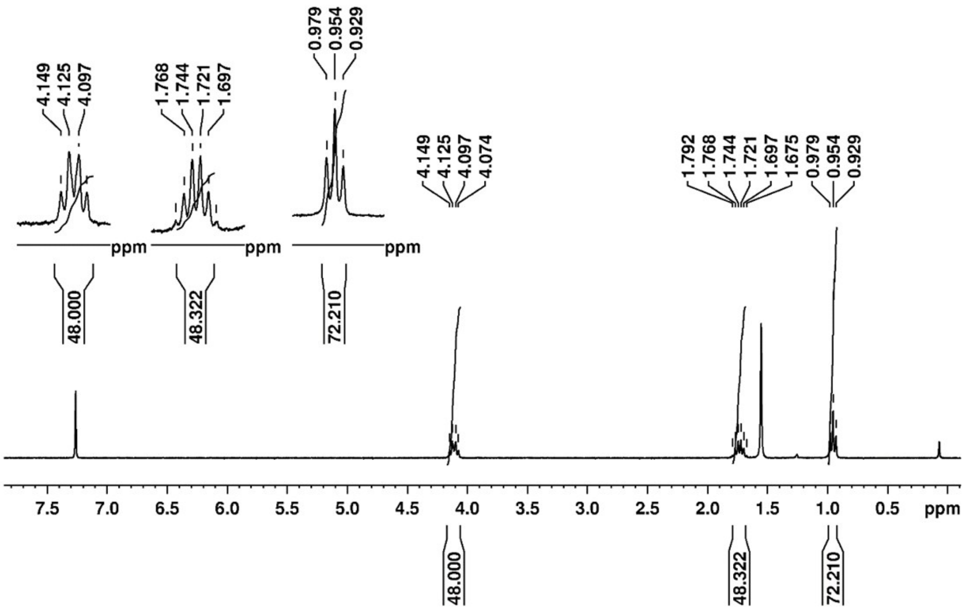

Figure S2. ^{1}H NMR spectrum of **1** (300 MHz, $CDCl_3$)

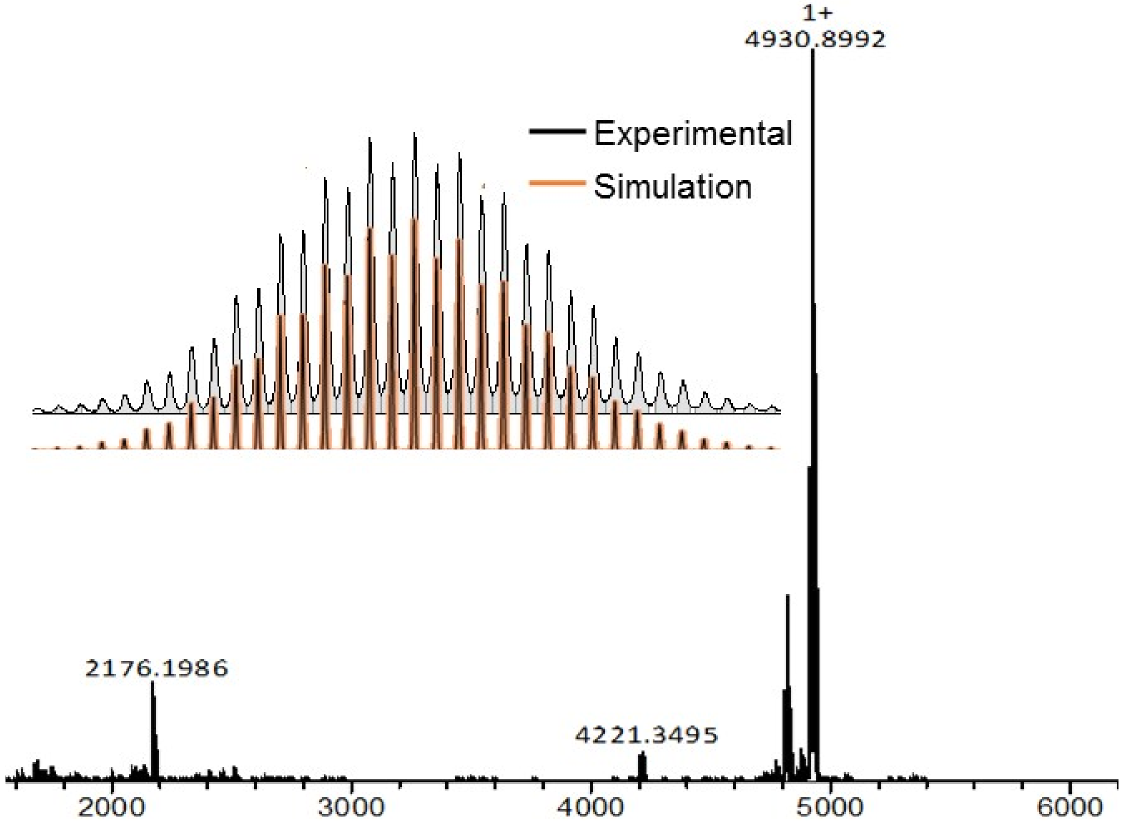

Figure S3. Positive mode ESI-MS of [**1**+Ag]$^+$. Insets: experimental (black) and simulated (red) mass spectra.

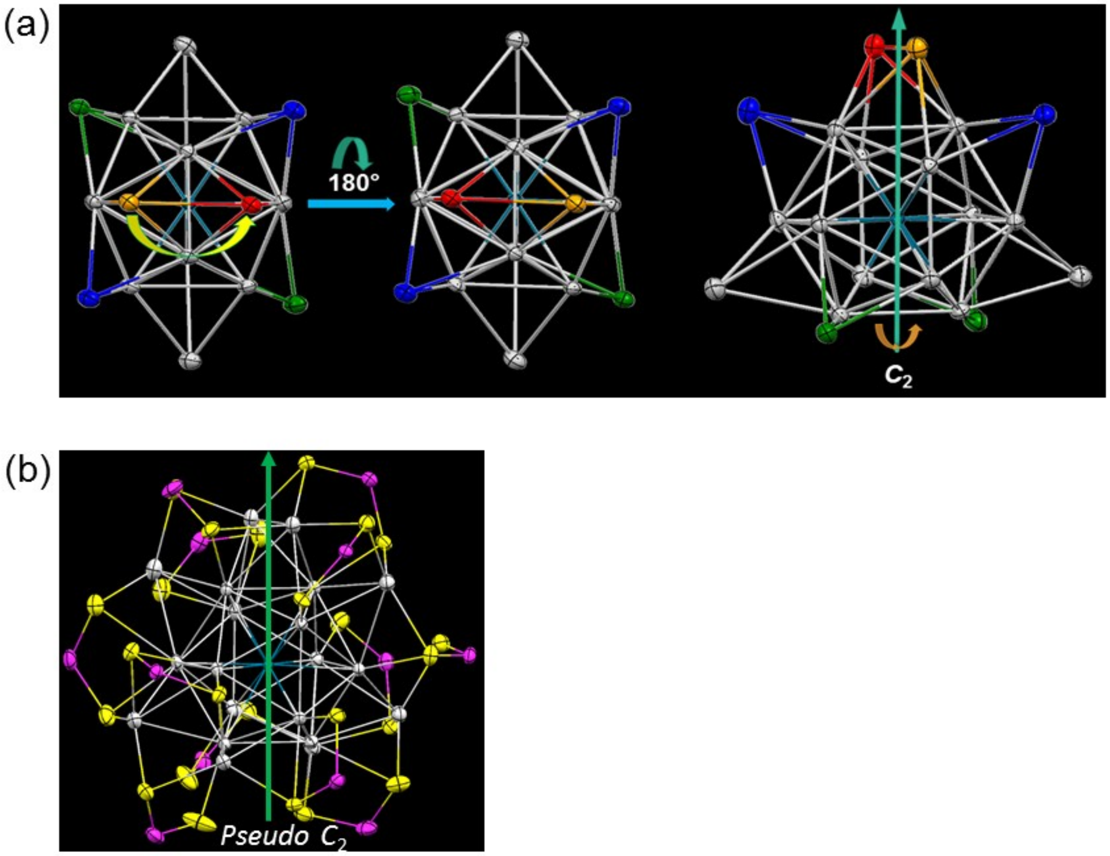

Figure S4. (a) Illustration of C_2 symmetry in the Pd@Ag_{12} core in **1**; capping Ag atoms are in different colors (color code. Pd: cyan; Ag_{ico}: gray, and Ag_{cap}: blue, green, orange, and red). (b) Dithiophosphate (dtp) ligands bind to the Ag atoms in three layers around the pseudo C_2 axis (color code. Pd: cyan; Ag: gray, P: pink, and S: yellow).

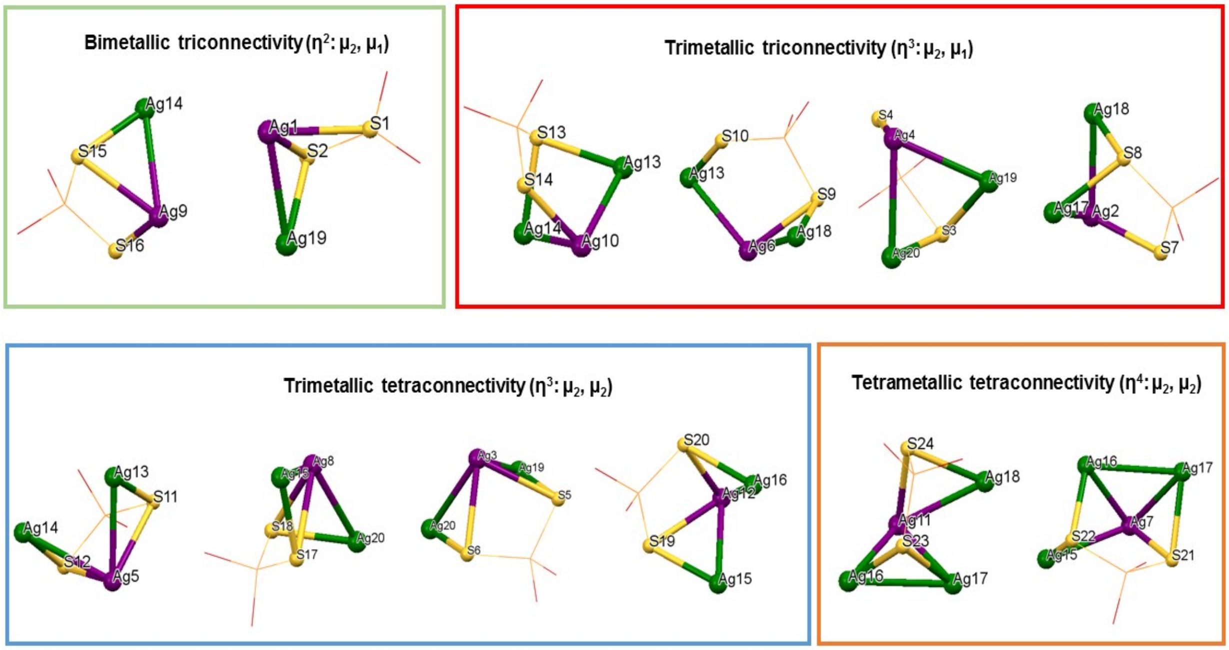
Bimetallic triconnectivity (η^2: μ_2, μ_1)

Trimetallic triconnectivity (η^3: μ_2, μ_1)

Trimetallic tetraconnectivity (η^3: μ_2, μ_2)

Tetrametallic tetraconnectivity (η^4: μ_2, μ_2)

Figure S5: Diffrent type of coordination modes of dithiophosphate (dtp) ligands in **1** (Color codes. Ag_{ico} : purple, Ag_{cap}: green, S:yellow, P: orange and O: red)

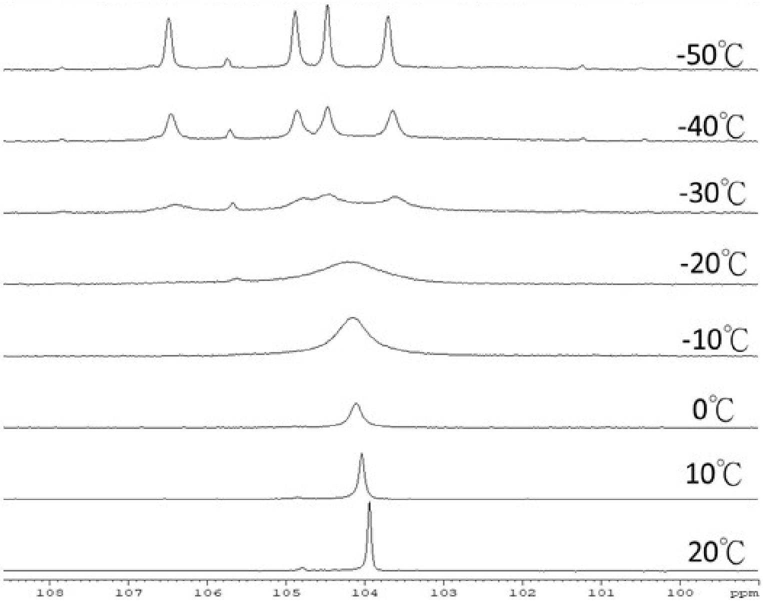

Figure S6: Variable temperature ^{31}P NMR spectrum of **1** (161.9 MHz, D_{6-}Acetone).

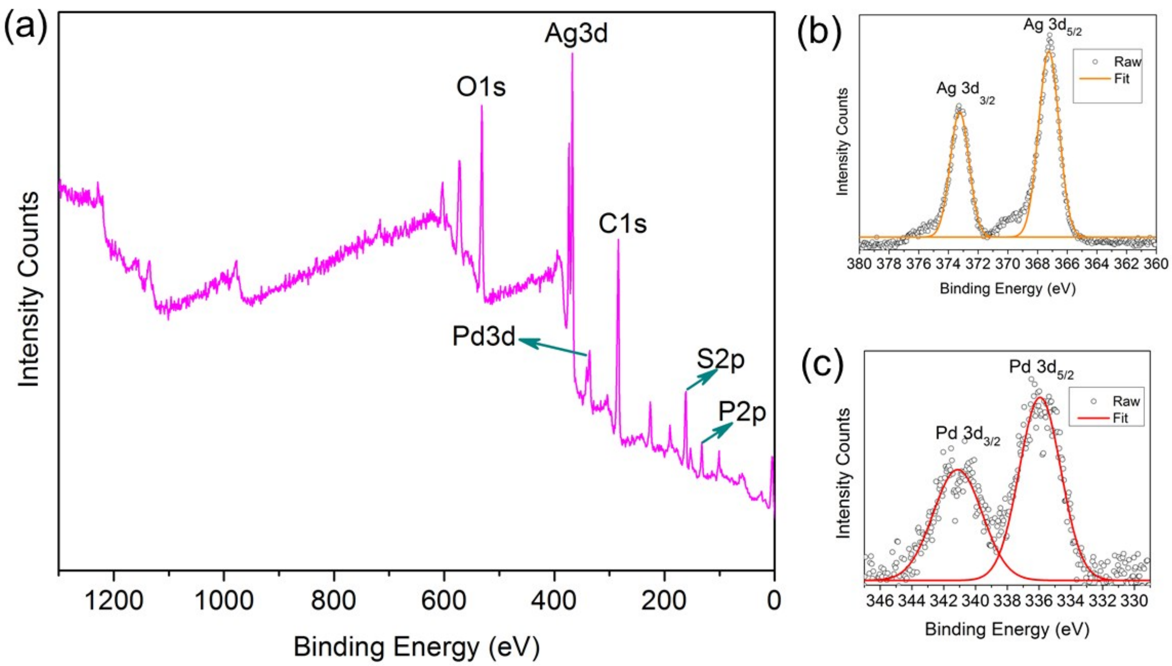

Figure S7. (a) XPS survey spectrum of **1**. (b) High resolution XPS spectrum of Ag in 3d region. (c) High resolution XPS spectrum of Pd in 3d region.

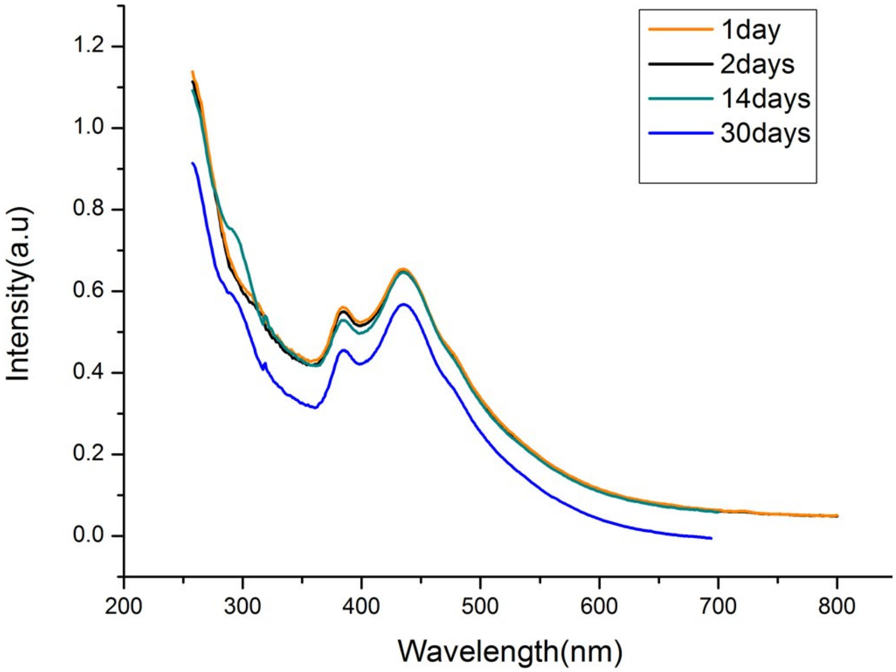

Figure S8: Time dependent UV–vis absorption study of **1** in 1 x 10^{-5} M CH_2Cl_2 solution and at room temperature.

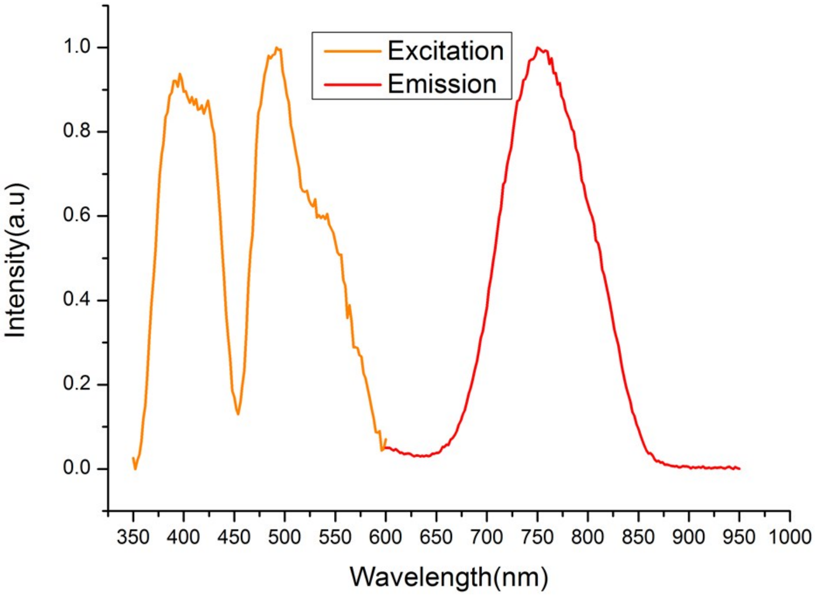

Figure S9. Excitation (left) and emission (right) spectra of compound **1** in MeTHF at 77K.

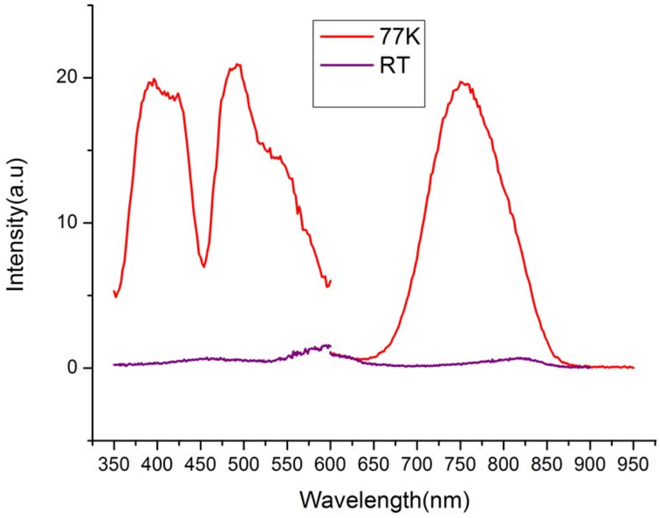

Figure S10: Variable temperature excitation and emission spectra of compounds **1** in MeTHF.

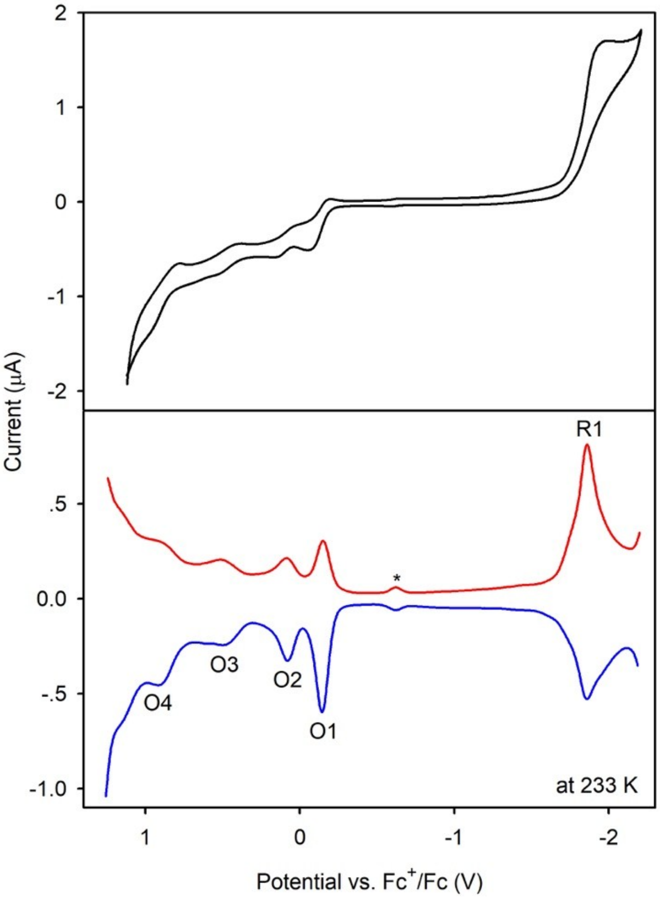

Figure S11: Cyclic voltammogram (top) and square wave voltammogram (bottom) of **1** recorded in CH_2Cl_2 at 233 K. Internal reference decamethylferrocene is denoted by an asterisk.

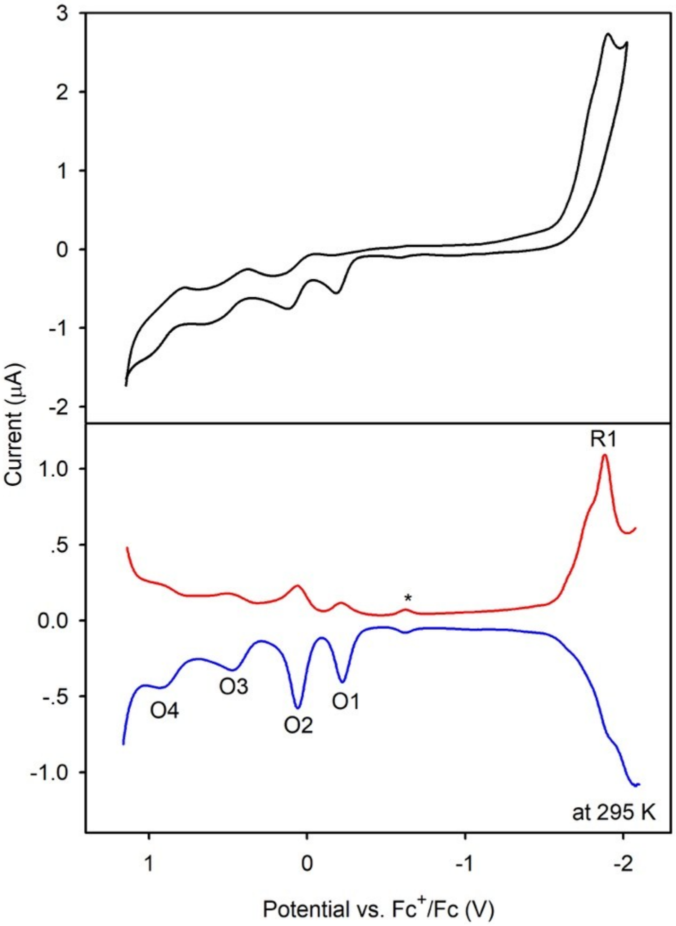

Figure S12: Cyclic voltammogram (top) and square wave voltammogram (bottom) of **1** recorded in CH_2Cl_2 at 295 K. Internal reference decamethylferrocene is denoted by an asterisk.

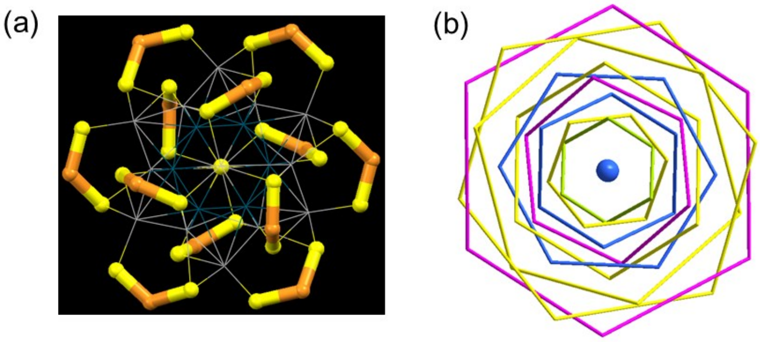

Figure S13: (a) Illustration of S_6 symmetry in **2** (color codes. Ag : grey, S:yellow, P: orange and Pd: bluegreen). (b) Layer by layer arrangement of ligand and metal atoms around the C_3 axis in **2** (color codes. Ag : blue, S:yellow, P: pink and Pd: green).

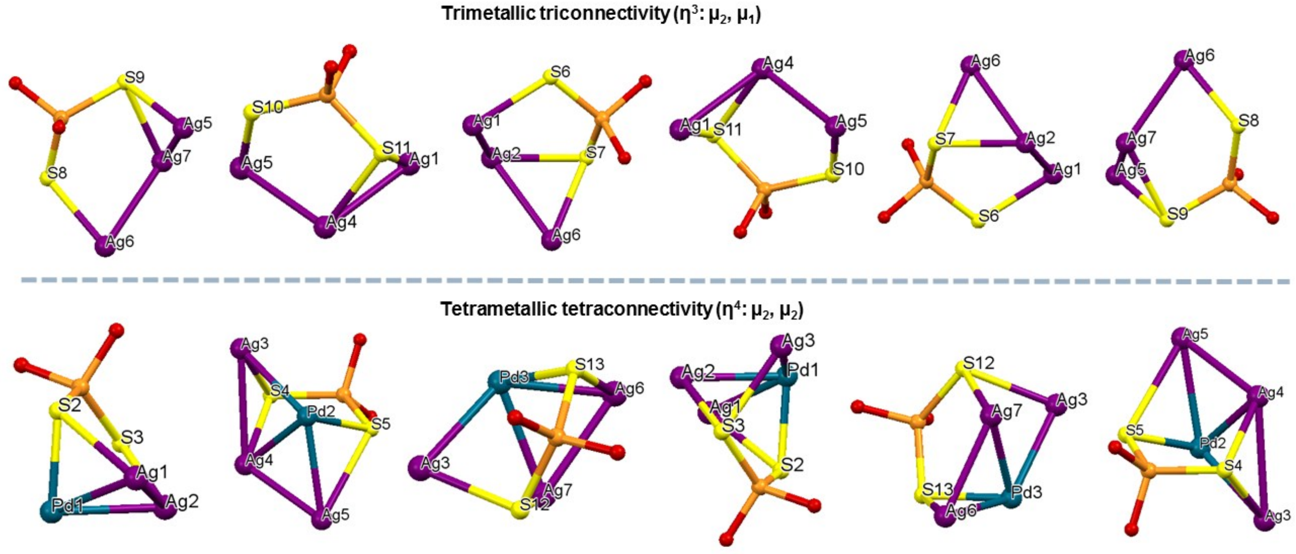

Figure S14: Diffrent type of coordination modes of dithiophosphate (dtp) ligands in **2** (Color codes. Ag_{ico} : purple, Ag_{cap}: green, S:yellow, P: orange and O: red).

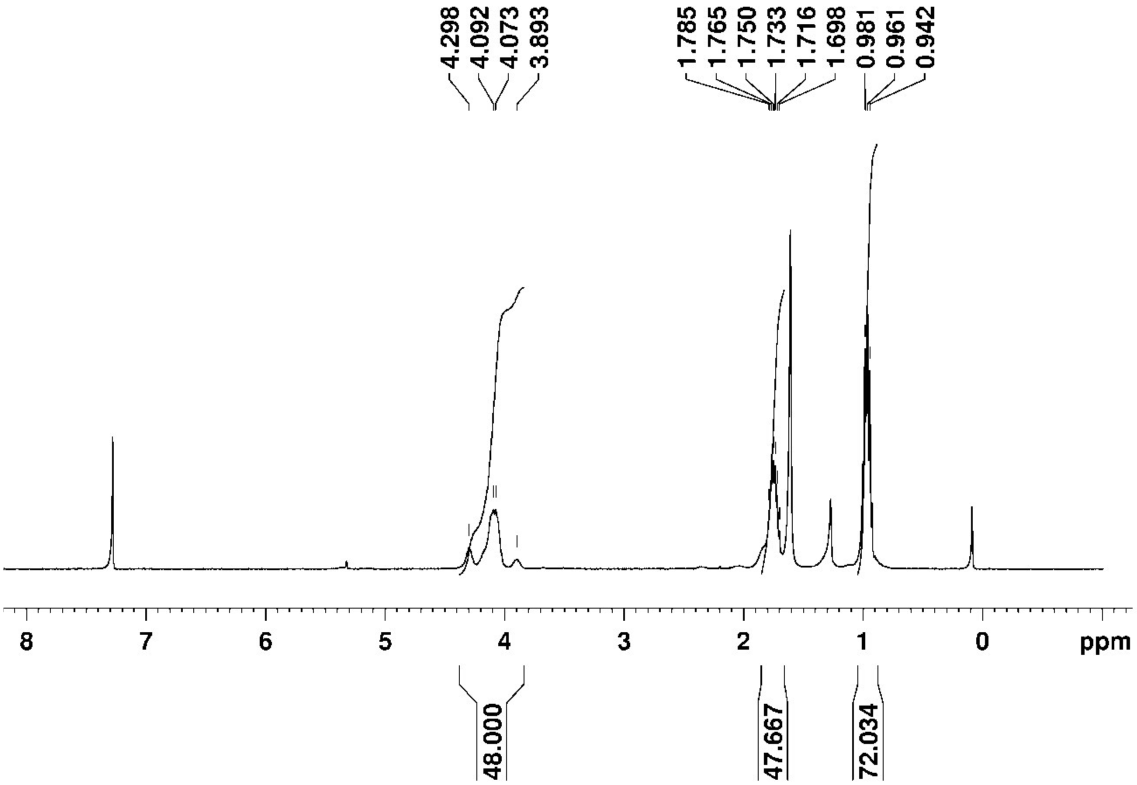

Figure S15: ^{1}H NMR spectrum of **2** (400 MHz, $CDCl_3$). NMR spectrum of **2**.

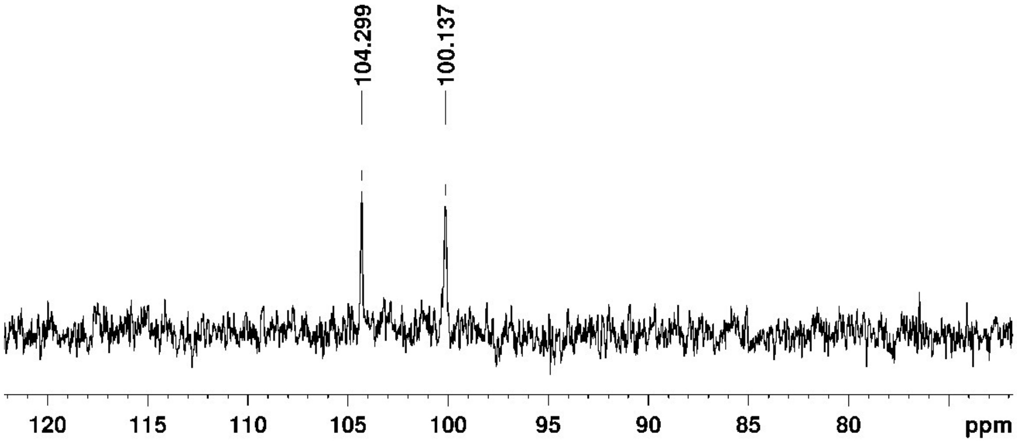

Figure S16: ^{31}P NMR spectrum of **2** (161.9 MHz, CDCl$_3$).

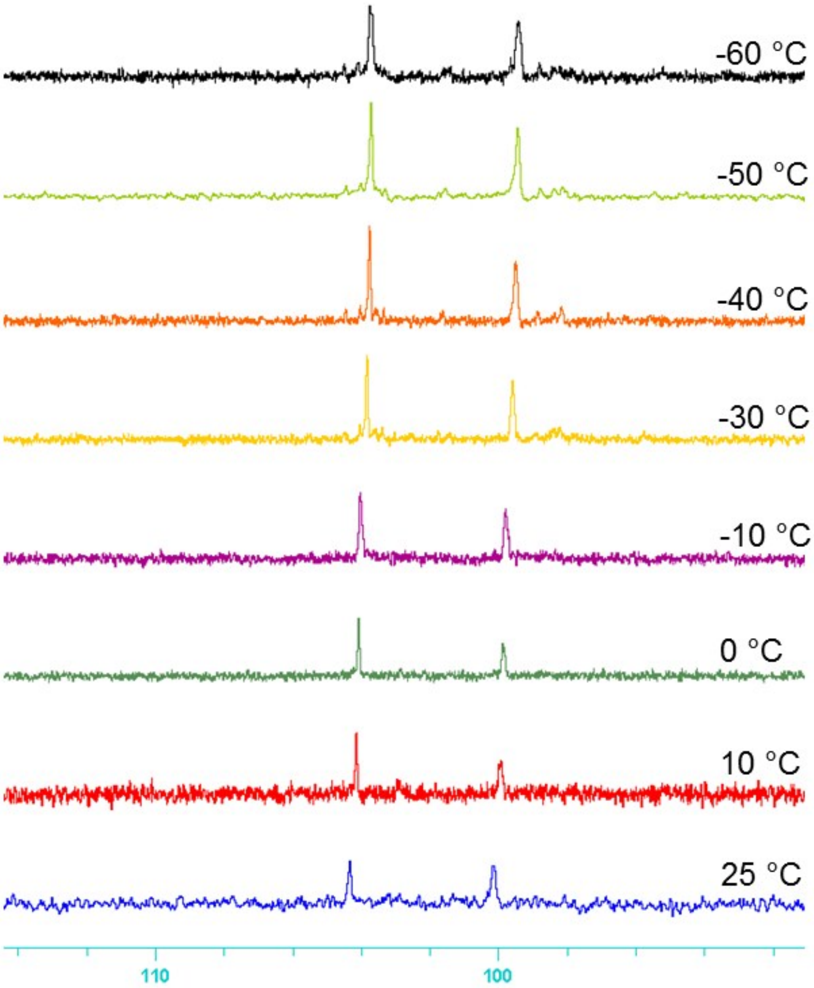

Figure S17: Variable temperature ^{31}P NMR spectrum of **2** (161.9 MHz, CDCl$_3$).

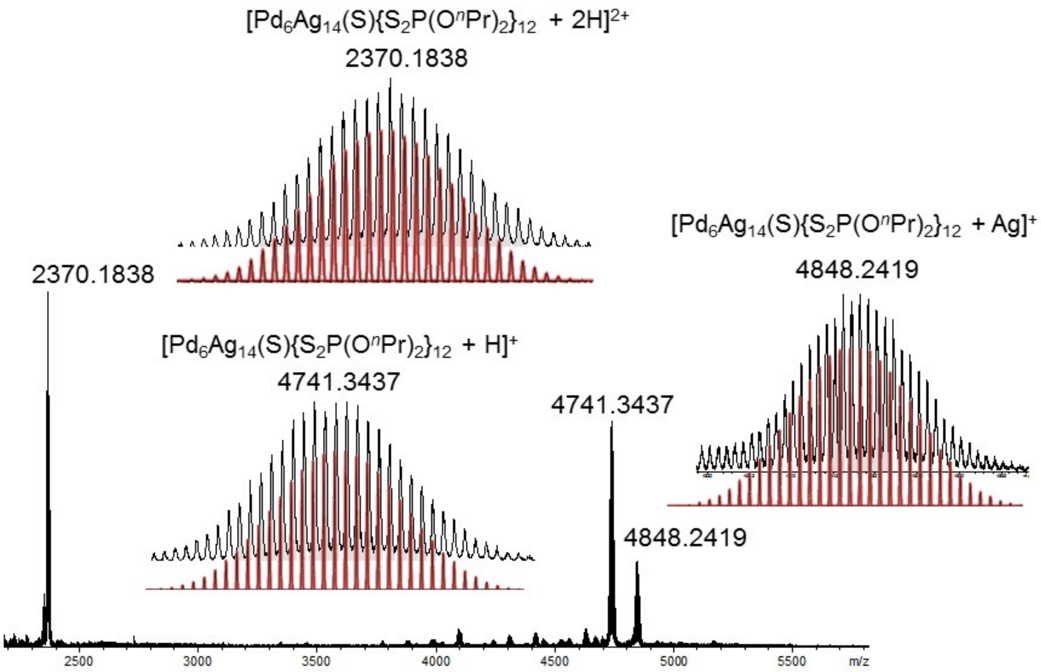

Figure S18: Positive ESI-MS spectrum of **2**. The inset shows the experimental (top) and theoretical spectra (bottom).

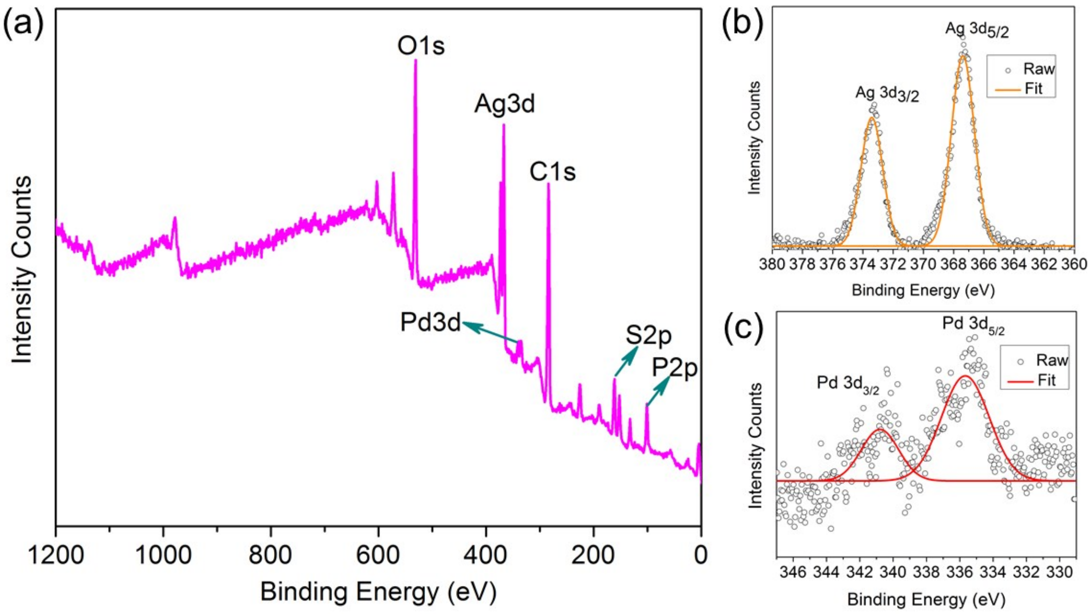

Figure S19. (a) XPS survey spectrum of **2**. (b) High resolution XPS spectrum of Ag in 3d region. (c) High resolution XPS spectrum of Pd in 3d region.

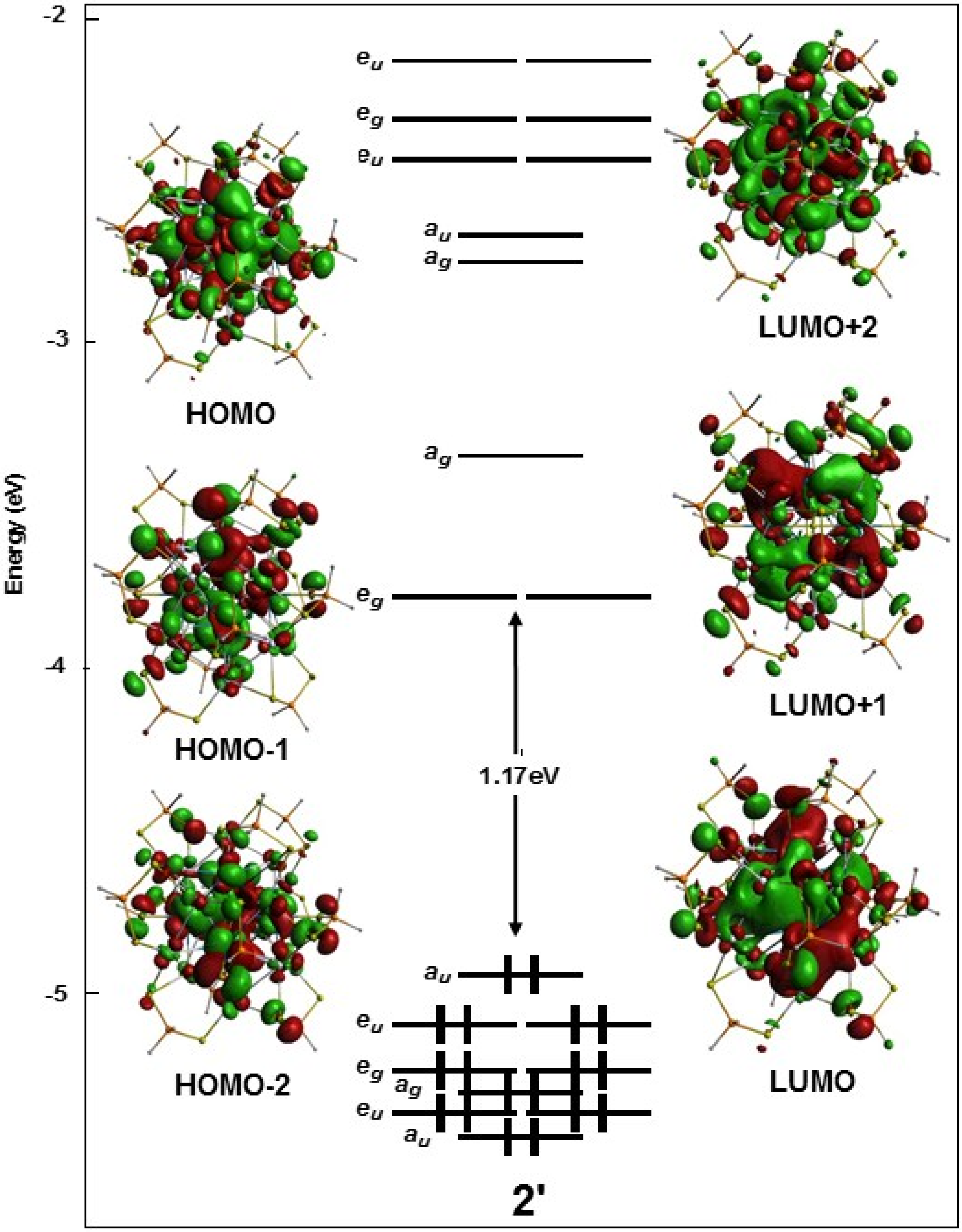

Figure S20. Kohn-Sham MO diagram of **2'** (S_6 symmetry).

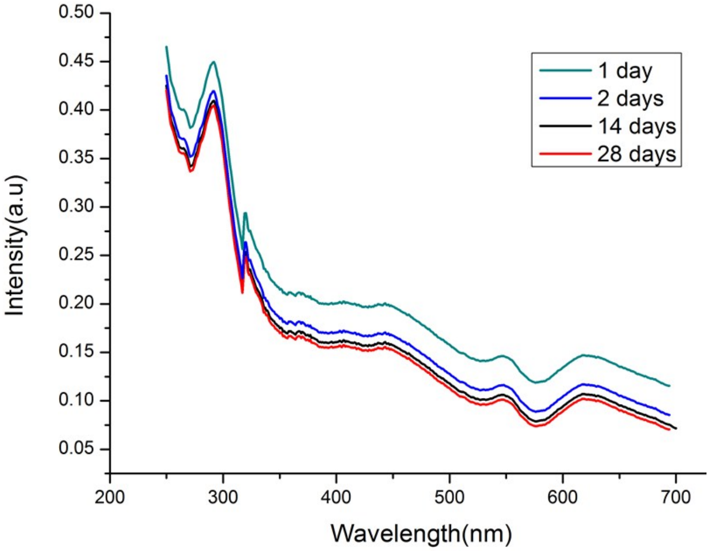

Figure S21: Time dependent UV–vis absorption study of **2** in 1 x 10^{-5} M CH_2Cl_2 solution and at room temperature.

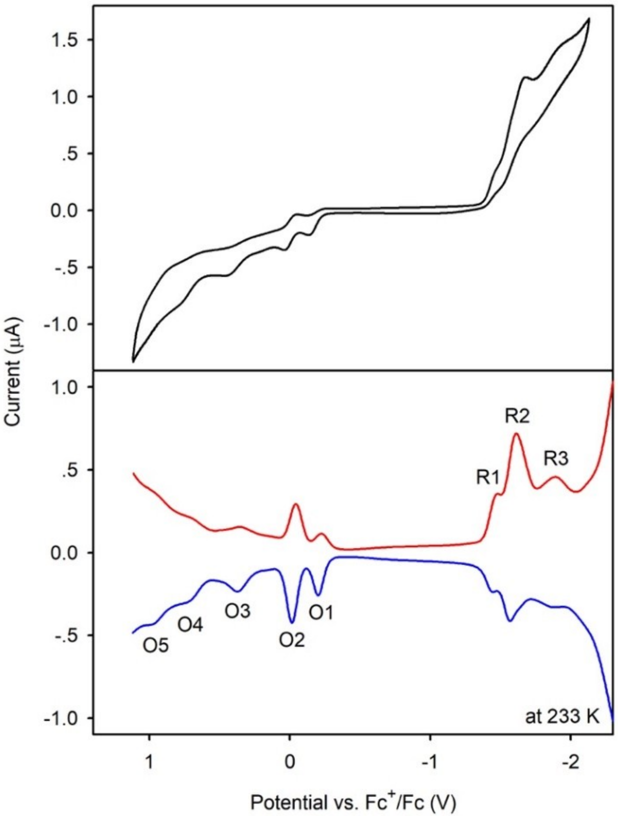

Figure S22: Cyclic voltammogram (top) and square wave voltammogram (bottom) of **2** recorded in CH_2Cl_2 at 233 K.

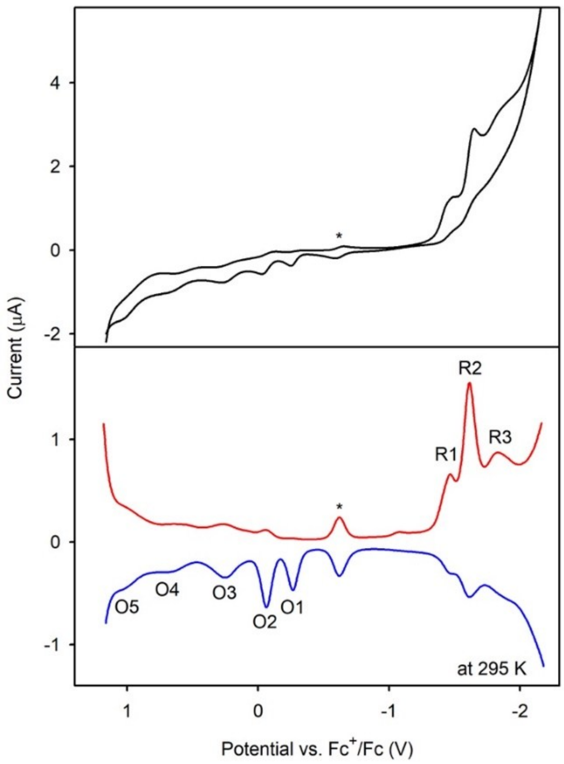

Figure S23: Cyclic voltammogram and square wave voltammogram of **2** recorded in CH_2Cl_2 at 295 K. Internal reference decamethylferrocene is denoted by an asterisk.

$$\begin{array}{c}
6[Pd^{2+} + 2Ag^0 \longrightarrow Pd^0 + 2Ag^+] \\
[S + 2Ag^0 \longrightarrow S^{2-} + 2Ag^+] \\
\hline
6Pd^{2+} + 14Ag^0 + S \longrightarrow 6Pd^0 + 14Ag^+ + S^{2-}
\end{array}$$

Figure S24: The plausible pathway of the formation of **2**.

Table S1: Crystallographic data for compounds **1** and **2**.

	1	**2**
CCDC	1911605	1911606
Empirical formula	$C_{75} H_{175} Ag_{20} O_{24} P_{12} Pd S_{24}$	$C_{72} H_{168} Ag_{14} O_{24} P_{12} Pd_6 S_{25}$
Formula weight	4866.02	4739.77
Crystal system, space group	Monoclinic, $P2_1/c$	Triclinic, $P\bar{1}$
a, Å	30.0622(12)	14.5737(7)
b, Å	17.3584(7)	17.0670(8)
c, Å	29.8055(12)	17.2156(8)
α, deg.	90	118.2870(10)
β, deg	109.4870(10)	92.2040(10)
γ, deg	90	105.1650(10)
Volume, Å^3	14662.5(10)	3572.3(3)
Z	4	1
ρ_{calcd}, g·cm^{-3}	2.204	2.203
μ, mm^{-1}	3.246	3.156
Temperature, K	150	150
θ_{max}, deg. / Completeness, %	25.000/99.7	25.000/99.7
Reflections collected / unique	84712 / 25747 [R(int) = 0.0376]	30013 / 12533 [R(int) = 0.0167]
restraints / parameters	400 / 1440	262 / 746
R1[a], wR2[b] [I > 2σ(I)]	R1 = 0.0387, wR2 = 0.0885	R1 = 0.0302, wR2 = 0.0675
R1[a], wR2[b] (all data)	R1 = 0.0520, wR2 = 0.0979	R1 = 0.0376, wR2 = 0.0735
Goodness of fit	1.035	1.03
Largest diff. peak and hole, e/Å ^{3}	2.286 and -1.710	1.629 and -0.991

Table S2: Relevant interatomic distances computed for **2'** without and with (in parentheses) the inclusion of the empirical GD3JB dispersion corrections.

Distances	Maximum	Minimum	Average
Ag-Ag	2.932 (3.188)	2.901 (2.858)	2.917 (2.996)
Pd-Pd	3.001 (2.902)	3.001 (2.902)	3.001 (2.902)
Ag-Pd	3.202 (3.073)	2.833 (2.758)	2.947 (2.849)
Pd-S_{center}	2.305 (2.280)	2.305 (2.280)	2.305 (2.280)
Ag-S	2.693 (3.012)	2.515 (2.485)	2.617 (2.694)
Pd-S	2.372 (2.375)	2.372 (2.375)	2.372 (2.375)

References:

(1) A. A. M. Alyl, B. Walfortn and H. *Z.* Lang, *Kristallogr. NCS,* 2004, **219**, 489-491.

(2) N. D. Yordanov, M. Ivanova, G. Gochev and J. Macicek, *Polyhedron*, 1993, **12**, 117-124.

(3) M. Gianini, W. R. Caseri, V. Gramlich and U. W. Suter, *Inorg. Chim. Acta*, 2000, **299**, 199-208.

(4) *SADABS*, version 2014-11.0, Bruker Area Detector Absorption Corrections (Bruker AXS Inc., Madison, WI, 2014).

(5) *SAINT*, included in G. Jogl, V4.043: Software for the CCD detector system (Bruker Analytical: Madison, WI, 1995).

(6) G. M. Sheldrick, *Acta Cryst. A,* 2008, **64**, 112-122.

(7) T. Gruene, H. W. Hahn, A. V. Luebben, F. Meilleur and G. M. Sheldrick, *J. Appl. Cryst.,* 2014, **47**, 462-466.

(8) *SHELXTL*, version 6.14. (Bruker AXS Inc., Madison, Wisconsin, USA, 2003).

(9) Gaussian 16, Revision B.01, M. J. Frisch, G. W. Trucks, H. B. Schlegel, G. E. Scuseria, M. A. Robb, J. R. Cheeseman, G. Scalmani, V. Barone, G. A. Petersson, H. Nakatsuji, X. Li, M. Caricato, A. V. Marenich, J. Bloino, B. G. Janesko, R. Gomperts, B. Mennucci, H. P. Hratchian, J. V. Ortiz, A. F. Izmaylov, J. L. Sonnenberg, D. Williams-Young, F. Ding, F. Lipparini, F. Egidi, J. Goings, B. Peng, A. Petrone, T. Henderson, D. Ranasinghe, V. G. Zakrzewski, J. Gao, N. Rega, G. Zheng, W. Liang, M. Hada, M. Ehara, K. Toyota, R.

Fukuda, J. Hasegawa, M. Ishida, T. Nakajima, Y. Honda, O. Kitao, H. Nakai, T. Vreven, K. Throssell, J. A. Montgomery, Jr., J. E. Peralta, F. Ogliaro, M. J. Bearpark, J. J. Heyd, E. N. Brothers, K. N. Kudin, V. N. Staroverov, T. A. Keith, R. Kobayashi, J. Normand, K. Raghavachari, A. P. Rendell, J. C. Burant, S. S. Iyengar, J. Tomasi, M. Cossi, J. M. Millam, M. Klene, C. Adamo, R. Cammi, J. W. Ochterski, R. L. Martin, K. Morokuma, O. Farkas, J. B. Foresman, D. J. Fox, Gaussian, Inc., Wallingford CT, 2016.

(10) (a) A. D. Becke, *Phys. Rev. A*, 1988, **38**, 3098-3100; (b) J. P. Perdew, *Phys. Rev. B*, 1986, **33**, 8822-8824.

(11) (a) A. Schaefer, H. Horn and R. Ahlrichs, *J. Chem. Phys.,* 1992, **97***,* 2571-77; (b) A. Schaefer, C. Huber and R. Ahlrichs, *J. Chem. Phys.,* 1994, 100, 5829-35.

(12) S. Grimme, S. Ehrlich and L. Goerigk, *J. Comp. Chem.,* 2011, **32**, 1456-1465.

(13) E. D. Glendening, J. K. Badenhoop, A. E. Reed, J. E. Carpenter, J. A. Bohmann, C. M. Morales, C. R. Landis and F. Weinhold, *NBO 6.0*; Theoretical Chemistry Institute, University of Wisconsin, Madison, WI, 2013**,** http://nbo6.chem.wisc.edu.

(14) (a) F. Weigend and R. Ahlrichs, *Phys. Chem. Chem. Phys*. 2005, **7**, 3297-3305; (b) F. Weigend, *Phys. Chem. Chem. Phys.,* 2006, **8***,* 1057-1065.

(15) (a) M. Cossi, V. Barone, R. Cammi and J. Tomasi, *Chem. Phys. Lett.* 1996, **255**, 327-335; (b) V. Barone, M. Cossi and J. Tomasi, *J. Chem. Phys.,* 1997, **107**, 3210-3221.

(16) T. Yanai, D. Tew and N. Handy, *Chem. Phys. Lett.,* 2004, **393**, 51-57.

(17) S. I. Gorelsky, SWizard program, revision 4.5, http://www.sg-chem.net.

(18) S. I. Gorelsky, AOMix program, http://www.sg-chem.net.